ARCHIVES OF ELECTRICAL ENGINEERING VOL. 72(4), pp. 1121 –1133 (2023)

DOI 10.24425/aee.2023.147430

A discrete variable based methodology for topology optimization considering spatially uneven manufacturing errors

MENG XIA, JING LI ✉

School of Information and Electrical Engineering, Hangzhou City University
Hangzhou, 310027, China
e-mail: {xiameng/✉lijing}@hzcu.edu.cn

(Received: 08.08.2023, revised: 05.10.2023)

Abstract: Manufacturing errors (MEs) are unavoidable in product fabrication. The omnipresence of manufacturing errors (MEs) in product engineering necessitates the development of robust optimization methodologies. In this research, a novel approach based on the morphological operations and interval field (MOIF) theory is proposed to address MEs in the discrete-variable-based topology optimization procedures. On the basis of a methodology for deterministic topology optimization (TO) based on the Min-Cut, MOIF introduces morphological operations to generate geometrical variations, while the dimension of the structuring element is dynamically set by the interval field function's output. The effectiveness of the proposed approach as a powerful tool for accounting for spatially uneven ME in the TOs has been demonstrated.

Key words: interval field, manufacturing errors, morphological operation, topology optimization

1. Introduction

Topology optimization (TO) is to optimize the distribution of materials within a device based on specific performance criteria during the initial phase of device design. Nowadays, TO has evolved to a novel paradigm, offering a quantitative design approach for devices design. In real-world devices, particularly microscale devices like antennas and MEMS (Micro Electronic Mechanical Systems), the inherent discrepancy between the computationally optimized topology and the actual built structure due to manufacturing tolerances can significantly impair the final

design's performance. Consequently, the exploration of robust optimization (RO) methods that account for manufacturing errors (ME) has emerged as a prominent and crucial topic in the field of the TO. By integrating the RO and the TO, researchers aim to develop design strategies that ensure the resilience of optimized topologies against manufacturing uncertainties, leading to more reliable and high-performing products in practical applications [1].

A critical concern in the ROME is the suitable representation of a topological deviation. In the solid isotropic material with penalization (SIMP) method, the projection threshold, which determines the filtering of the element density in the deterministic TO, is represented by a random field in the robust TO to represent MEs [2, 3]. In the level set method (LSM), a perturbation function $\delta(x, \theta)$ is added to the original level set function $\varphi(x, \theta)$ in the deterministic TO, so that the boundary of ME is represented by the modified zero level set of a perturbed LSF $\varphi(x, \theta)$ [4].

The aforementioned methodologies for the ROME suffer from two major issues. Firstly, it is widely acknowledged that two distinct modeling approaches, namely discrete-variable-based and continuous-variable-based approaches, are universally employed in the TOs. In the continuous-variable-based approach, the design variable representing the status of each element is treated as a continuous value ranging from zero to one. This approach often involves material interpolation schemes to ultimately penalize the intermediate variable, forcing it into either the solid (one) or void (zero) status. On the other hand, the discrete-variable-based methodology describes design variables as discrete entities. Each of these two categories of methodologies has its unique advantages and disadvantages. However, the prevailing strategies for addressing the ROME in the field of TO are predominantly tailored to the continuous-variable-based modeling methodology, including the SIMP and the LSF, while negligible efforts have been paid to the ROME in the discrete-variable-based TO. A continuous-variable-based TO method basically represents the geometrical deformation by disturbing the intermediate variables, and is obviously inapplicable to a discrete-variable-based modelling one.

Secondly, most techniques developed for the ROME are probability-based approach, such as random field model, which requires a large amount of information for the accurate description of the probability parameters. Nevertheless, the accurate probability parameters of the uncertainties, such as the mean and the standard deviation, are hard to predict in the initial phase of the design process. In contrast with the probability-based approach, the interval-based method employs solely the nominal value and the bounds of the uncertainties, operating independently of substantial prior information.

In this regard, this paper proposes a new technique for the ROME in discrete-variable-based TOs. A novel methodology for TOs based on Min-Cut [5] has been recently introduced and has demonstrated a remarkable capacity to generate new holes while effectively curbing the emergence of checkerboard patterns in the TO. By extending this work, an approach based on the morphological operations and interval field (MOIF) is firstly introduced to solve a discretely modelled TO problem considering MEs. Particularly, the geometrical deformation is treated as the fluctuation of the interface between two materials, and is represented using the morphological operations conducted on the computationally optimized topology. The dimension of the morphological operator is defined as the outcome of an interval field, allowing the MOIF to effectively represent spatially uneven MEs without the acquirement of large amount of information. The numerical results have validated the ability of the MOIF to generate optimized topologies capable of enduring the MEs.

2. Min-Cut based deterministic TO

2.1. The optimal direction change

The main concern of a TO problem is to determine the optimal redistribution of materials in each iteration. The quality of the optimized outcomes is predominantly assessed through two crucial indicators: piecewise smoothness and accuracy. In the context of a Min-Cut based approach, these indicators, piecewise smoothness and accuracy, are jointly evaluated through the utilization of the energy function [6]:

$$\begin{aligned}\min\colon E(X_0 \to X) &= -\left(\sum_{\{p,q\}\in N} S_{p,q}\left(X_p, X_q\right) + \sum_{p\in P} D_p\left(X_p\right)\right) \\ &= -\left(K \sum_{\{p,q\}\in N} \text{Connection}_{(p,q)} + \sum_{p\in P} SE_{X_p}(p)\right),\end{aligned} \tag{1}$$

where: $X_0 \to X$ indicates the direction change from topology X_0 to X, K stands for the weight, P represents a set of elements, X_p signifies the updated material attribute of element p determined by cut C, N denotes a set of the interacting pairs of elements, and connection correspond to the degree of connections defined as:

$$\text{Connection}_{(p,q)} = \begin{cases} 1 & p \text{ and } q \text{ are connected} \\ 0 & \text{otherwise} \end{cases}. \tag{2}$$

When considering two materials α and β to be redistributed (α possesses higher material property), the calibrated sensitivity $SE_{X_p}(p)$ is defined as:

$$SE_\alpha^p = \begin{cases} |se^p|, & se < 0 \\ -|se^p|, & se > 0 \end{cases}, \qquad SE_\beta^p = \begin{cases} -|se^p|, & se < 0 \\ |se^p|, & se < 0 \end{cases}, \tag{3}$$

where se signifies the original sensitivity concerning the objective function (typically computed using the adjoint variable method), while SE_α denotes the probability that an element is designated as α. For an element possessing material property α, a negative sensitivity se implies an elevation in the attribute parameter of the element, and vice versa. Given the minimization nature of the energy function, the element that ought to transit from α to β is characterised by a positive SE_α and a negative SE_β.

Evidently, minimizing the energy function will lead to a decrease in the variation of material distribution between a pair of interconnected elements featuring a significant connectivity level. Furthermore, the parameter K holds influence over the optimized outcomes. It is apparent that a smaller K barely constrains the emergence of checkerboard patterns. Nonetheless, an extensive spectrum of K values has been demonstrated to be effective [5].

2.2. Finding optimal direction using Min-Cut

For a weighted network, denoted as $G(V, E)$, as showed in Fig. 1, with two distinguished vertices "s" and "t", an s-t cut pertains to a collection of edges. The removal of these edges

results in the separation of G into two distinct segments while also placing "s" and "t" in separate portions within the residual graph $G(C) = (V, E - C)$ [6].

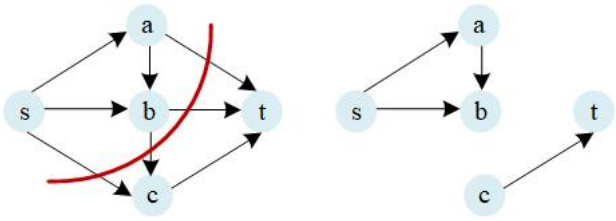

Fig. 1. An example of an s-t cut

To employ the Min-Cut theorem in a TO, the mesh-grid in the finite element analysis is initially converted into a network. One approach for this transformation is illustrated in Fig. 2(a). Subsequently, for a TO problem involving the reassignment of materials α and β, two terminals, labeled "α" and "β", are introduced into the primary network (as depicted in Fig. 2(b)). In the context of a TO problem, an s-t cut refers to a collection of edges whose removal leads to the disconnection of the network. Within the partitioned network, each element is exclusively connected to either "α" and "β". In simpler terms, an optimal direction is distinctly represented by an s-t cut in the transformed network. The relationship between cut C and the material assignment in the topology can be described as follows:

$$X_p^c = \begin{cases} \alpha & \text{if } t_p^\alpha \in C \\ \beta & \text{if } t_p^\beta \in C \end{cases} \quad \forall p \in P, \tag{4}$$

where X_p^c represents the modified material attribute of element p determined by cut C. The guidelines for the calculation of edge weights are detailed in [6].

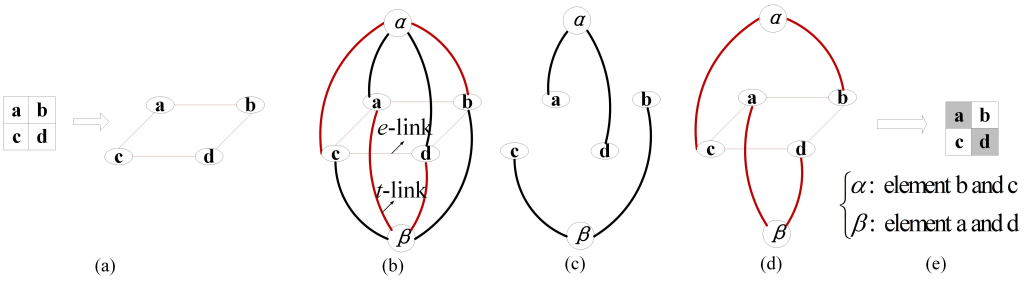

Fig. 2. A cut in the network for TOs: (a) one way of transformation of a mesh-grid into a network; (b) transformed network; (c) partitioned network; (d) cut set, and (e) updated material distribution

Furthermore, it has been established that the cost of a cut, denoted as $|C|$, which is the sum of the edge weights, is equivalent to the energy function [6]. As a result, the minimization of the energy function outlined in Eq. (1) is tantamount to identifying the Min-Cut within the transformed weighted network.

3. Manufacturing error representation using morphological operations and random field

3.1. Representation of manufacturing errors using morphological operations

Morphological operations, fundamental techniques in image processing, involve the application of a structuring element (SE) as a probe to a given binary image, resulting in the generation of a new image [7]. The SE is represented by a binary matrix. The dimensions of the matrix and the arrangement of ones and zeros within it determine the size and shape of the SE, respectively. The SE is consecutively positioned at every pixel within the image and matched against the corresponding pixel neighborhood. As depicted in Fig. 3, the SE is considered to fit the image if, for each of its pixels with a value of 1, the corresponding image pixel also holds a value of 1. Similarly, an SE is deemed to hit an image if, at least one of its pixels with a value of 1 aligns with a corresponding image pixel of value 1.

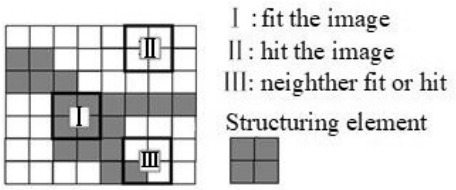

Fig. 3. Probing of an image with a SE (white and grey pixels present non-zero and zero values, respectively)

Erosion and dilation are foundational morphological operations. Following an erosion, the values at positions (x, y) within the resulting image C become 1 if the structuring element B fits within the corresponding area of A; otherwise, they become 0. Similarly, following a dilation, the values at positions (x, y) in the new image C become 1 if the structuring element B hits the corresponding region of A; otherwise, they become 0. The definitions of dilation and erosion are given as follows:

$$X \oplus H = \left\{(x, y) \colon H_{(x,y)} \cap X \neq \emptyset\right\}, \tag{5}$$

$$X - H = \{(x, y) \colon H_{(x,y)} \subseteq X\}. \tag{6}$$

Figure 4 provides a visual representation of the outcomes of erosion and dilation on an image utilizing a diamond-shaped structuring element. Evidently, the configuration and the dimensions of the structuring element collaboratively influence the pattern observed in the resultant image.

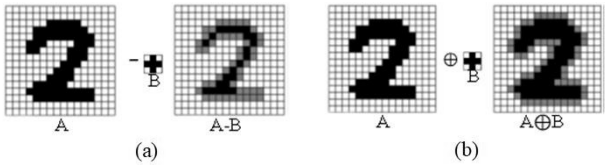

Fig. 4. Erosion operation (a); dilation operation (b)

In a discrete-variable-based TO, MEs can be conceptualized as rearranging 0/1 patterns within the boundary's vicinity. Put differently, specific portions of the material exhibit a propensity to expand, while others tend to contract. Consequently, it becomes logical to signify material growth through a dilation operation and material contraction through an erosion operation.

3.2. Interval field

Practically, the manufacturing tolerance often exhibit spatial variations. Moreover, the exact probability information is generally unavailable in the initial phase of the device design. Therefore, the interval field theory is employed to produce a spatially uneven geometrical deviation. The interval field theory utilizes the bounds of the variations to effectively describe spatial uncertainty. These bounds are typically more accessible in practical engineering.

A spatial uncertainty $H(\boldsymbol{u})$ is deemed an interval field when, for a given spatial location $\boldsymbol{u}_k \in \Delta$, $k = 1, 2, \ldots$, the potential values of $H(\boldsymbol{u}_k)$ can be depicted by an interval $H^I(\boldsymbol{u}_k) = [H^L(\boldsymbol{u}_k), H^U(\boldsymbol{u}_k)]$, wherein Δ signifies a bounded domain of the spatial location $\boldsymbol{u}$ [10, 11].

Considering an interval field $\{H(\boldsymbol{u}) \in H^I(\boldsymbol{u}_k), \boldsymbol{u} \in \Delta\}$, where $H^U(\boldsymbol{u})$ and $H^L(\boldsymbol{u})$ represent the upper and the lower bound function, its radius function $H^r(\boldsymbol{u})$ and midpoint function $H^m(\boldsymbol{u})$ are given as:

$$H^m(\boldsymbol{u}) = \frac{H^U(\boldsymbol{u}) + H^L(\boldsymbol{u})}{2}, \qquad H^r(\boldsymbol{u}) = \frac{H^U(\boldsymbol{u}) - H^L(\boldsymbol{u})}{2}. \tag{7}$$

The potential realizations of an interval field are strictly situated between the lower bound function $H^L(\boldsymbol{u})$ and the upper bound function $H^U(\boldsymbol{u})$. Figure 5 illustrates the comparison between the realizations of random field and the interval field. It is evident that, for each realization of the interval field, the fluctuation of $H(\boldsymbol{u}_k)$ is rigorously confined to $H^I(\boldsymbol{u}_k) = [H^L(\boldsymbol{u}_k), H^U(\boldsymbol{u}_k)]$, whereas the realizations of the random field cannot be ensured to locate within the interval.

It is generally hoped to represent a spatial uncertainty using a set of uncorrelated variables. In this regard, the widely recognized Karhunen–Loève (K–L) expansion theorem is utilized in this

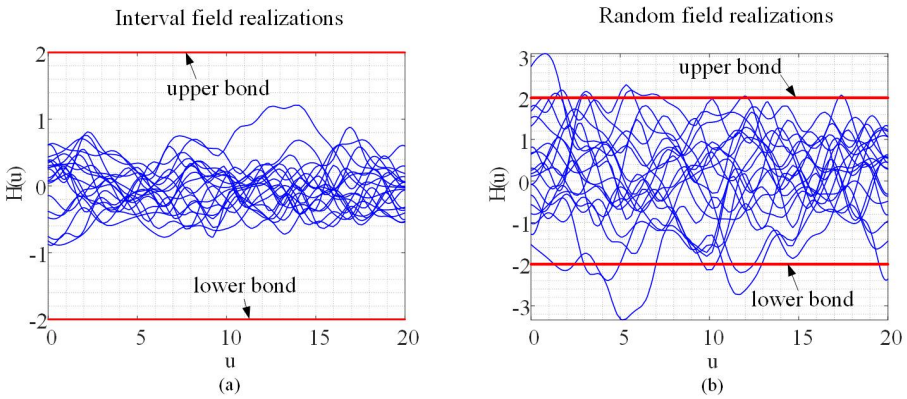

Fig. 5. Realizations of an interval field (a); a random field (b)

article to depict a spatially continuous interval field using sets of orthogonal deterministic basis functions featuring uncorrelated interval coefficients.

An interval field $H(\boldsymbol{u})$ is expressed using K–L expansion [8, 9] as:

$$H(\boldsymbol{u}) = H^m(\boldsymbol{u}) + \sum_{j=1}^{\infty} H^r(\boldsymbol{u})\sqrt{\lambda_j}\varphi_j(\boldsymbol{u})\xi_j\,, \quad \xi_j \in [-1, 1], \tag{8}$$

where $H^r(\boldsymbol{u})$ and $H^m(\boldsymbol{u})$ correspond to the radius function and the midpoint function of the interval field, respectively. The uncorrelated interval variables are denoted as $\xi_j \in \xi^I = [-1,\ 1]$, $j = 1, 2, \ldots$, which satisfy $\sum_{j=1}^{\infty} \xi^2 \leq 1$. The eigenvectors and the eigenvalues are denoted as $\psi_j(\boldsymbol{u})$ and $\lambda_j \in [0, \infty]$, respectively.

In general, a significant portion of the attributes associated with a spatial uncertainty can be effectively captured by the principal terms. In terms of practical application, approximating interval field uncertainty involves arranging the eigenvalues λ_j in descending order and limiting the expansion to the first$M$ terms. As a result, a truncated Karhunen–Loève expansion can be defined as follows:

$$H(\boldsymbol{u}) = H^m(\boldsymbol{u}) + \sum_{j=1}^{M} H^r(\boldsymbol{u})\sqrt{\lambda_j}\varphi_j(\boldsymbol{u})\xi_j\,. \tag{9}$$

Given an interval field, both the radius function $Hr(\boldsymbol{u})$ and the midpoint function $H^m(\boldsymbol{u})$ are predetermined. Consequently, following Eq. (9), the primary objective in the approximation of such an interval field using the interval Karhunen–Loève expansion lies in the computation of eigenvalues λ_j and eigenfunctions $\psi_j(\boldsymbol{u})$, which could be acquired through solving the subsequent Fredholm integral equation of the second kind:

$$\int_D C(\boldsymbol{u}_1, \boldsymbol{u}_2)\varphi_j(\boldsymbol{u}_1)\,\mathrm{d}\boldsymbol{u}_1 = \lambda_j\varphi_j(\boldsymbol{u}_2). \tag{10}$$

In this study, a squared exponential covariance function is used:

$$C(\boldsymbol{u}_1, \boldsymbol{u}_2) = e^{-|u_1 - u_2|/L}, \tag{11}$$

where L is the correlation length.

Many numerical methods have been proposed to solve Eq. (10) [10, 11]. After obtaining λ_j and the $\psi_j(\boldsymbol{u})$, the interval field could therefore be approximated using Eq. (9).

3.3. Quantification of manufacturing errors using interval field and morphological operator

The goal of the TO is to redistribute the material in the design domain to achieve optimal device performance. Therefore, the manufacturing tolerance of the TO could be regarded as the deformation of the interface between different materials. Moreover, the variation of the interface in a 2D problem could be depicted by an interval field of one dimension.

To employ the interval field interval field $\{H(\boldsymbol{u}) \in H^I(\boldsymbol{u}_k), \boldsymbol{u} \in \Delta\}$ for the representation of the nonuniform variation of the interface within the given range, the interface to be conducted

should firstly be extracted. The integral interval in Eq. (6) is discretized into K segments, which is equal to the number of the elements contained in the interface. In each realization of $H(\boldsymbol{u})$, a vector h containing K interval variables will be generated. As showed in Fig. 6, for the i-th element on the interface, a morphological operation with an SE (suppose a square shaped one) of the length equal to $H(\boldsymbol{u}_k)$ will be operated. Specifically, a positive diameter indicates a dilation, whereas a negative diameter signifies an erosion.

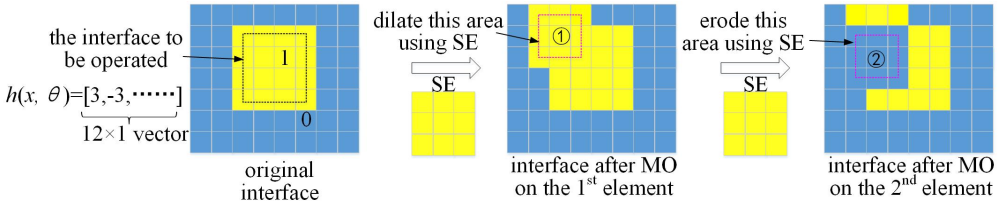

Fig. 6. Illustration of dilation and erosion based on interval field

Figures 7(a)–7(c) show the original material distribution (white is air and black is iron), the extracted interface of the material, and the neighborhood of the interface where the deformations will take place, respectively. Figure 8 depicts four deformed interfaces under the four realizations of the $H(\boldsymbol{u})$ illustrated in Fig. 9.

Fig. 7. The original material distribution (a); the extracted interface of the material (b); the neighborhood of the interface (c)

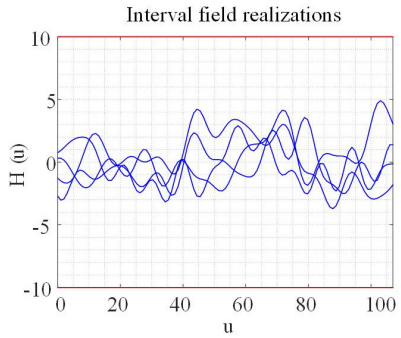

Fig. 8. Four realizations of the $H(\boldsymbol{u})$

Moreover, the form of the deformation is associated with the correlation length L of the interval field. The lower the correlation length, the more frequent the deformation is. Therefore,

Fig. 9. Four deformed interfaces

the correlation length determines the shape of the deformation. Figures 10(a) and 10(b) show the realizations of interface deformation under lower correlation length and the higher one, respectively. By tuning the value of the correlation length, one can represent the geometrical deformation of different shapes more practically.

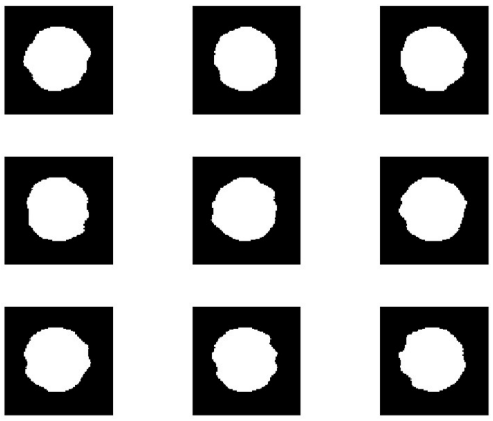

(a)

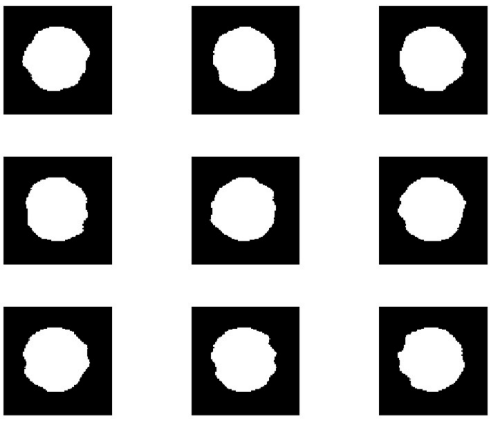

(b)

Fig. 10. Geometrical variations under correlation $L = 25$ (a) and $L = 50$ (b)

4. Numerical results

To validate the proposed methodology, a magnetic actuator comprising a coil, a yoke, and an armature [12] is topologically optimized to enhance the magnetic force in a specific direction. In the finite element analysis, the design domain is discretized into a grid of 30×9 quadrilateral elements. The coils, consisting of 400 turns, are subject to an input current of 1 A. The deterministic objective function is defined as:

$$\begin{aligned} &\text{Minimize } f = \frac{\partial W_{\text{magnetic}}}{\partial x}, \\ &\text{Subject to } g = \sum_{e=1}^{270} \frac{V^e}{V_0 - V_{\text{set}}} < 0, \quad V^e = \begin{cases} 1, & \text{element } e \text{ is iron} \\ 0, & \text{element } e \text{ is air} \end{cases}. \end{aligned} \tag{12}$$

The robust equivalents of the deterministic objective function f and the constraint function g within interval uncertainty are characterized by their worst-case scenarios, defined as follows:

$$\begin{aligned} f_w(x,\delta) &= \underset{(\delta_N - \delta_0 \le \delta \le \delta_N + \delta_0)}{\text{Max}} [f(x,\delta)], \\ g_w(x,\delta) &= \underset{(\delta_N - \delta_0 \le \delta \le \delta_N + \delta_0)}{\text{Max}} [g(x,\delta)]. \end{aligned} \tag{13}$$

In this numerical example, the midpoint function is set as: $H^m(\boldsymbol{u}) = 0$, indicating that the geometrical deformations fluctuate around the original interface. The radius function is set as $H^r(\boldsymbol{u}) = 8$, indicating that the width of the neighborhood where the fluctuations occur is set 5 (evaluated by the number of elements in the mesh-grid). The correlation length is set 5. During each optimization iteration, 40 realizations of $H(\boldsymbol{u})$ are conducted, resulting in the need to compute the sensitivity of each element 40 times. Obviously, the computational burden is comparatively higher than that of the deterministic TO. It should be noted that the primary emphasis of robust optimization lies in the quantification and propagation of the uncertainties. However, the focus of this article is on the quantification of the manufacturing uncertainty in the TO, without delving into the computation of uncertain propagation. Further research remains imperative to delve into the propagation of geometric uncertainty, thereby reducing the computational cost of topology optimization problems considering the manufacturing errors.

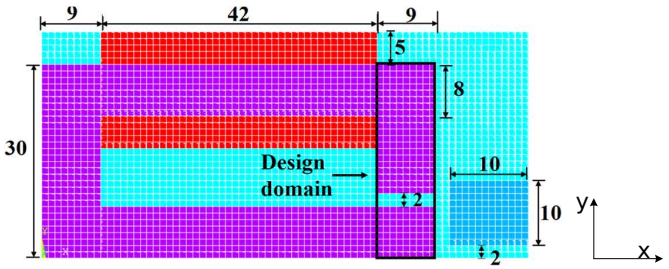

Fig. 11. Schematic diagram of the actuator

Figure 12(a) displays the outcomes of deterministic topology optimization, while Fig. 12(b) exhibits the results of robust topology optimization (areas in black signify air). The magnetic

forces of the optimized topology obtained from the deterministic optimization and the robust one are –55.62 N/m and –52.82 N/m, respectively. A comparison between the two reveals that, in the deterministic optimized topology, the air region (black) located at the lower left corner of the design domain is notably slender and susceptible to contraction due to geometric uncertainty (as depicted in Fig. 12(c)). Consequently, this can lead to the obstruction of the magnetic flux towards the armature, resulting in a substantial decline in magnetic force. Conversely, in the robust optimized topology, this area expands, rendering it less susceptible to the effects of geometry uncertainty.

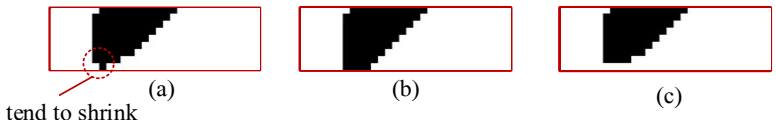

Fig. 12. Optimized topology from deterministic optimization (a); optimized topology from robust optimization (b); distorted topology from (a) (c)

To test the ability of the robustly optimized results to withstand MEs, some post experiments are conducted on the topologies in Figs. 13(a) and 13(b), respectively. To be specific, 20 realizations of $H(\boldsymbol{u})$, with the midpoint function $H^m(\boldsymbol{u}) = 0$ and the radius function $H^r(\boldsymbol{u}) = 4$, are generated to represent the manufacturing errors conducted on the topologies in Figs. 12(a) and 12(b). Figures 13(a) and 13(b) illustrate the magnetic force of each topology with varies geometries. The mean and standard deviation of the magnetic force are tabulated in Table 1.

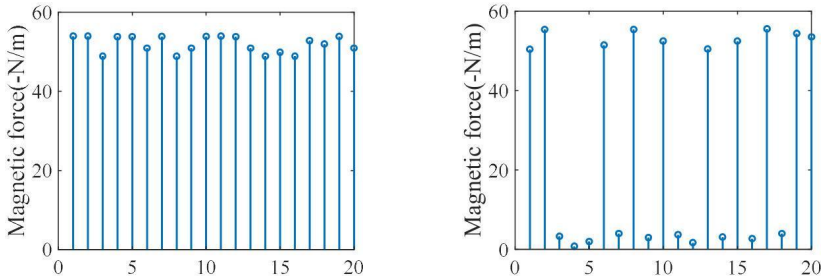

Fig. 13. Performance variance of the test experiments on robust optimized topology (a) and deterministic optimized topology (b)

Table 1. The results of the post experiment

	Expected value of the magnetic force (N/m)	**Standard deviation of the magnetic force**
Deterministic result	–28	668
Robust result	–51.97	4.21

Evidently, the optimized topology under robust optimization demonstrates a notable resilience to geometric uncertainties.

5. Conclusions

This study extends the Min-Cut based methodology for the discrete-variable-based TO to a TO considering spatially uneven manufacturing errors by introducing an interval field and morphological operations to appropriately represent a spatially uneven geometry deviations. The key advantage of the MOIF lies in its ability to rigorously quantify spatially nonuniform MEs in the TO with limited prior information, thereby enhancing the resilience of the optimized topologies. The numerical results have demonstrated that the proposed method is capable of generating optimized topologies that exhibit the ability to withstand the effects of geometric uncertainty.

Acknowledgements

This research was supported by the Natural Science Foundation of China under Grant 52207017, the State Key Laboratory of Reliability and Intelligence of Electrical Equipment No. EERI_KF2021006, Hebei University of Technology, and Zhejiang Provincial Natural Science Foundation of China under Grant No. LY21F030002.

References

[1] Kostina M., Karaulova T., Sahno J. *et al.*, *Reliability estimation for manufacturing processes*, Journal of Achievements in Materials and Manufacturing Engineering, vol. 51, pp. 7–13 (2012), DOI: 10.5755/j01.mech.18.6.3168.

[2] da Silva G.A., Beck A.T., Sigmund O., *Topology optimization of compliant mechanisms with stress constraints and manufacturing error robustness*, Computer Methods in Applied Mechanics and Engineering, vol. 354, pp. 397–421 (2019), DOI: 10.1016/j.cma.2019.05.046.

[3] da Silva G.A., Beck A.T., Sigmund O., *Stress-constrained topology optimization considering uniform manufacturing uncertainties*, Computer Methods in Applied Mechanics and Engineering, vol. 344, pp. 512–537 (2019), DOI: 10.1016/j.cma.2018.10.020.

[4] Wang Li-Luan *et al.*, *Non-probabilistic Reliability-based Topology Optimization (NRBTO) Scheme for Continuum Structures Based on the parameterized Level-Set method and Interval Mathematics*, Computer Methods in Applied Mechanics and Engineering, vol. 373, 113477 (2021), DOI: 10.1016/j.cma.2020.113477.

[5] Xia M., Yang S., Sykulski J., *A Novel 3D Topology Optimization Methodology based on the Min-Cut Theorem*, IEEE Transactions on Magnetics, vol. 57, pp. 1–5 (2021), DOI: 10.1109/TMAG.2021.3075015.

[6] Kolmogorov V., Zabih R., *What Energy Functions Can Be Minimized via Graph Cuts*, IEEE Transactions on Pattern Analysis and Machine Intelligence, vol. 26, pp. 147–159 (2004), DOI: 10.1109/TPAMI.2004.1262177.

[7] Comer M.L., Delp III E.J., *Morphological operations for color image processing*, Journal of Electronic Imaging, vol. 8, pp. 279–289 (1999), DOI: 10.1117/1.482677.

[8] Ni B.Y., Jiang C., *Interval field model and interval finite element analysis*, Science Direct, Computer Methods in Applied Mechanics and Engineering, vol. 360, pp. 1–40 (2020), DOI: 10.1016/j.cma.2019.112713.

[9] Wu J.L., Zhen Luo, Nong Zhang, Zhang Y.Q., *A new uncertain analysis method and its application in vehicle dynamics*, Mechanical Systems and Signal Processing, vol. 50, pp. 659–675 (2015), DOI: 10.1016/j.ymssp.2014.05.036.

[10] Phoon K.K., Huang S.P., Quek S.T., *Simulation of second-order processes using Karhunen–Loève expansion*, Computers & Structures, vol. 80, pp. 1049–1060 (2002), DOI: 10.1016/S0045-7949(02)00064-0.

[11] Babolian Esmail, Jafar Biazar, Vahidi A.R., *The decomposition method applied to systems of Fredholm integral equations of the second kind*, Applied Mathematics and Computation, vol. 148, no. 2, pp. 443–452 (2004), DOI: 10.1016/S0096-3003(02)00859-7.

[12] Xia M., Zhou Q., Sykulski J., Yang S., Ma Y., *A Multi-Objective Topology Optimization Methodology Based on Pareto Optimal Min-Cut*, IEEE Transactions on Magnetics, vol. 56, pp. 1–5 (2020), DOI: 10.1109/TMAG.2019.2955386.